



Research paper

Cooperative luminescence mediated near infrared photocatalysis of $\text{CaF}_2:\text{Yb}$ @ BiVO_4 composites

Xiaohui Liu, Weihua Di*, Weiping Qin*

State Key Laboratory on Integrated Optoelectronics, College of Electronic Science and Engineering, Jilin University, Changchun, 130012, China

ARTICLE INFO

Article history:

Received 31 August 2016

Received in revised form 13 October 2016

Accepted 7 December 2016

Available online 10 December 2016

Keywords:

Photocatalysis

Near infrared

Photocatalytic activity

Cooperative luminescence

Energy transfer

ABSTRACT

It is a challenge to develop efficient photocatalyst that can be activated by photons with long wavelength. In our previous work, a near infrared (NIR) driven photocatalyst (e.g., $\text{NaYF}_4:\text{Yb,Tm@TiO}_2$) was designed, for which, however, a two-step energy transfer was involved for photocatalysis so that the ultimate photocatalytic capability is low. In this work, we designed and prepared a new type of NIR photocatalyst composed of cooperative luminescence agent $\text{CaF}_2:\text{Yb}$ and semiconductor BiVO_4 , in which a one-step energy transfer occurs to realize NIR photocatalysis. Steady-state and dynamic fluorescence spectroscopy analysis revealed that cooperative energy transfer of a Yb^{3+} -dimer to BiVO_4 leads to the indirect excitation of semiconductor BiVO_4 by NIR light. The degradation of methylene blue (MB) compound by $\text{CaF}_2:1\%\text{Yb}^{3+}@\text{BiVO}_4$ particles upon NIR radiation and its corresponding controlled experiments demonstrated the NIR light responsive photocatalytic capability. It is noteworthy that nearly 80% degradation ratio of MB was achieved with 7 h of NIR light irradiation, indicating a relatively high photocatalytic activity, compared with that of our previously reported system $\text{NaYF}_4:\text{Yb,Tm@TiO}_2$, for which ~65% of degradation ratio of MB was obtained within 14 h of NIR irradiation. Recycling experiments of photocatalysis indicate that our present $\text{CaF}_2:\text{Yb}@\text{BiVO}_4$ composite has good photochemical stability in spite of a long time of NIR irradiation.

© 2016 Elsevier B.V. All rights reserved.

1. Introduction

Photocatalysis is an economical and environmentally friendly technique that can be applied in environmental remediation, solar energy conversion, and organic photosynthesis [1–5]. Since Fujishima and Honda discovered the photocatalytic water-splitting on crystalline TiO_2 electrodes for hydrogen production in 1972 [6], research interests in TiO_2 photocatalysis have grown significantly owing to its strong oxidizing power under ultraviolet (UV) light, extraordinary chemical stability, as well as environmental friendly and biocompatible features [7–15]. However, TiO_2 with crystalline anatase phase has a bandgap of ~3.2 eV, and mainly absorbs UV light [16], which accounts for only about 5% of the incoming solar energy. Therefore, visible and infrared photons with energy lower than the bandgap energy of TiO_2 , which occupies more than 90% of the solar energy, cannot be harvested for photocatalysis [17,18].

To address this problem, much effort has been devoted to extending the absorption of TiO_2 to the long wavelength region for efficient use of solar energy. To reach this goal, several strategies have been proposed by adjusting the bandgap toward visible light

energies through the introduction of noble metals, cationic substitutions, and anionic doping [19–27]. Although the absorption of TiO_2 by these modification methods could be adjusted to the visible region, the overall catalytic capability was found to decrease due to an increased recombination of photogenerated electrons and holes [28–30]. Therefore, it is still a challenge to find an appropriate way to extend the absorption of TiO_2 to visible and NIR region.

Recently, our group has first reported the activation of broadband semiconductor by NIR phonons for photocatalysis via combining upconverting luminescence agent $\text{YF}_3:\text{Yb,Tm}$ and semiconductor TiO_2 to construct a core-shell structure, in which $\text{YF}_3:\text{Yb,Tm}$ acts as a mediate for converting NIR to UV light via a multiphoton upconversion process [31]. In the subsequent work, we investigated the energy transfer process between upconverting luminescent agent and semiconductor by steady-state and dynamic fluorescence spectroscopy, and revealed that the fluorescence resonant energy transfer dominated for NIR photocatalysis in such a core-shell structure [32]. Later, our idea of activating broadband semiconductor by NIR photons has been transplanted and applied in the areas of H_2 production via water splitting [33,34], photovoltaic device [35,36] and photodynamic therapy [37–39] by other research groups.

Indeed, there exists a two-step energy transfer for realizing NIR-responsive photocatalysis in our previously designed catalytic

* Corresponding authors at: 2699 Qianjin Street, Changchun, 130012, China.
E-mail addresses: whdi@jlu.edu.cn (W. Di), wpqin@jlu.edu.cn (W. Qin).

material, i.e., Yb^{3+} – Tm^{3+} energy transfer first, and then Tm^{3+} – TiO_2 energy transfer. As we have known, multiple-step energy transfer would increase the loss of photo energy significantly and reduce the ultimate efficiency of energy transfer to TiO_2 largely, resulting in a low photo quantum yield for exciting TiO_2 . Therefore, it seems a promising strategy to reduce the energy transfer procedures for improving the photo quantum efficiency of exciting TiO_2 , and thus increasing the NIR-light responsive photocatalytic activities.

Cooperative luminescence refers to a process by which a pair of ions emits one photon by simultaneous depopulation from their excited states [40–42]. The cooperative luminescence of a pair of excited Yb^{3+} -ions was first observed in 1970 [40]. Very recently, our group has reported the cooperative luminescence involving three neighboring Yb^{3+} -ions in CaF_2 host, in which the UV emission is observed under NIR excitation [43]. Clearly, the cooperative luminescence shows a novel upconversion luminescent mechanism, for which the energy transfer process is not involved. In this work, guided by this special upconversion luminescence mechanism, we designed a new type of NIR-activatable photocatalytic material by combining a typical cooperative luminescence agent CaF_2 : Yb and a well-known semiconductor BiVO_4 , in which NIR light photocatalysis was achieved via a one-step energy transfer process. Due to the reduction of energy transfer procedures for our present catalytic material in this work, the photocatalytic activity was improved remarkably, compared with that of our previously reported NIR-responsive catalytic system (e.g., NaFY_4 : Yb , Tm @ TiO_2) [32].

2. Experimental

2.1. Preparation of CaF_2 : 1% Yb^{3+}

The powder sample of CaF_2 : 1% Yb^{3+} was prepared using a high temperature solid-state reaction method. The raw materials CaF_2 and YbF_3 were thoroughly mixed by grinding together, and then heated up to 1400°C for 2 h in an argon atmosphere and quenched to room temperature.

2.2. Preparation of CaF_2 : 1% Yb @ BiVO_4

The CaF_2 : Yb @ BiVO_4 composite was prepared by a conventional co-precipitation method. In a typical process, 0.5 mmol as-prepared CaF_2 : 1% Yb and 0.1 mmol $\text{Bi}(\text{NO}_3)_3$ · $5\text{H}_2\text{O}$ were dispersed into 10 mL HNO_3 solution (2 M), and 0.1 mmol NH_4VO_3 was dispersed into 10 mL NH_3 · H_2O solution (2 M) under violent stirring. Then, the solution containing $\text{Bi}(\text{NO}_3)_3$ and CaF_2 : 1% Yb was added to the NH_4VO_3 solution slowly under violent stirring. After stirring for 3 h, the pH of the mixed solution was adjusted to 7 using NH_3 · H_2O solution and then the mixed solution was kept stirring for another 12 h to get a homogeneous solution. The obtained solution was transferred into a 20 mL stainless autoclave with a Teflon liner and then the stainless autoclave was maintained at 180°C for 24 h. After cooling down to room temperature naturally, the obtained products were washed with MiliQ water and ethanol for three times, respectively. The obtained samples were dried in 70°C for 24 h in a drying oven. For comparison, we prepared the CaF_2 : Yb @ BiVO_4 composites with different CaF_2 : Yb -to- BiVO_4 molar ratios (10:0.5, 10:1, 10:2, 10:3, 10:4, respectively).

2.3. Characterization

The purity and phase structure of the resulting products were analyzed with a Model Rigaku Ru-200b X-ray powder diffractometer (XRD) using a nickel-filtered $\text{Cu-K}\alpha$ radiation ($\lambda = 1.5406\text{\AA}$) in the 2-Theta ranging from 10° to 70° . Field-emission scanning electron microscopy (SEM) images were recorded using a JEOL

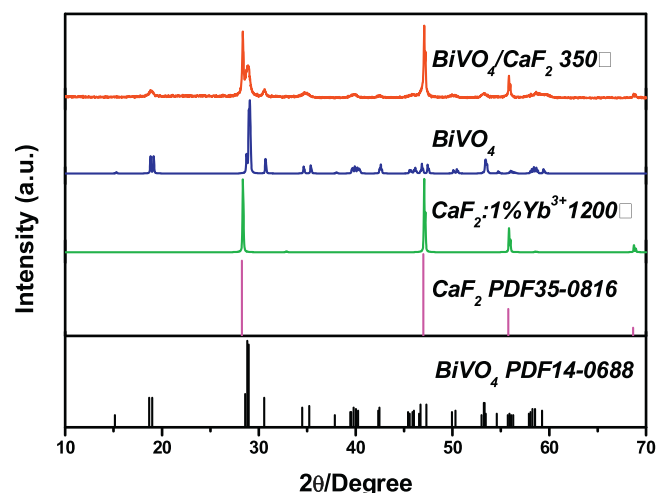


Fig. 1. XRD patterns of CaF_2 : Yb with and without BiVO_4 deposition. Standard XRD patterns of JCPDS 35-0816 (CaF_2) and 14-0688 (BiVO_4) are also shown.

JSM-7500F microscope operating at 5 kV at a working distance of 2–3 mm. For the SEM observations, samples were prepared without any carbon coating simply by depositing some powder onto a silicon slice. The UV-vis-NIR diffuse reflectance spectrum was recorded with a Shimadzu UV-3600 in the wavelength ranged of 200–1000 nm, using BaSO_4 for background scanning. Raman spectra were recorded at room temperature using a LabRAM HR evolution Raman spectrometer (HORIBA Scientific) in the back-scattering geometry with a 532 nm semiconductor as an excitation source. Power-adjustable continuous wave laser diodes (978 nm, 10 W, BWT Beijing Ltd, Beijing, China) were employed as the pump sources for spectral analysis. The luminescence spectra were recorded with an 1-m monochromator (SPEX 1000 M, model: 232/488MSD; HORIBA Jobin Yvon Inc., Edison, NJ, USA) equipped with a 1800 lines mm^{-1} for visible fluorescence grating. A digital oscilloscope (DPO4104B, bandwidth 1 GHz, sampling rate 5 GSs $^{-1}$; Tektronix, Shanghai, China), a power-adjustable continuous wave laser diode (CW978 nm, 10 W), and a chopper were used to record decay curves.

2.4. Photocatalytic experiments

The photocatalysis was performed with NIR irradiation in the presence of photocatalyst using methyl blue (MB) as a model pollutant. The degradation of MB was evaluated by measuring its optical absorption using a Shimadzu UV-3600 spectrophotometer. In a typical experiment, 0.5 mg of CaF_2 : Yb @ BiVO_4 particles was dispersed into a quartz cuvette containing 0.5 mL of MB aqueous solution (15 mg L^{-1}), and then kept in the dark prior to irradiation for establishing adsorption-desorption equilibrium of MB on the surface of CaF_2 : Yb @ BiVO_4 particles before irradiation. A diode laser of 980 nm with a power of 10 W/cm^2 was used as the irradiation source. After irradiation of 980 nm light for a designated time, 0.3 mL of MB aqueous solution was taken out for UV-vis absorbance measurements, and then put back into the quartz corvette. The concentration of MB solution at each time interval was calculated using the calibration curve of the standard solution.

3. Results and discussion

3.1. Phase and morphological characterization

Fig. 1 shows the XRD pattern of the product obtained via high temperature sintering of CaF_2 and YbF_3 mixtures at Ar atmo-

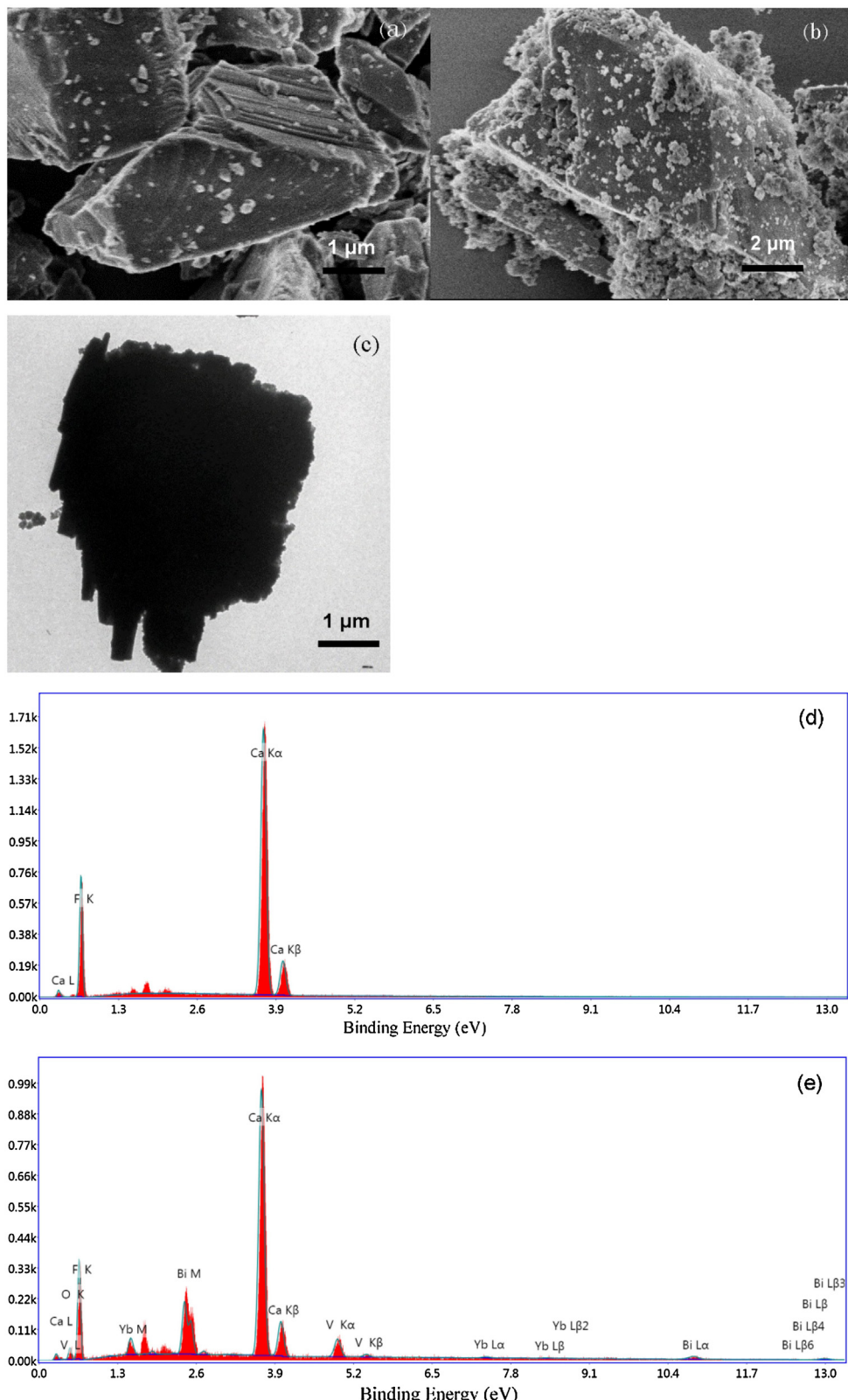


Fig. 2. SEM (a, b) and TEM images (c) and EDX spectra (d, e) of $\text{CaF}_2\text{:Yb}$ and $\text{CaF}_2\text{:Yb@BiVO}_4$ composites.

sphere. The position and relative intensity of all diffraction peaks can be readily indexed to cubic CaF_2 phase, compared with the JCPDS file NO. 35-0816. No impurity was detected, indicating that the as-prepared product was single-phased. The particle size and morphology of Yb-doped CaF_2 phosphors were investigated

through SEM. Fig. 2(a) presents a typical SEM image of as-prepared $\text{CaF}_2\text{:1\%Yb}$ phosphors, in which large particles with the size of 5–10 μm are observed.

Upon the addition of $\text{Bi}(\text{NO}_3)_3$ and NH_4VO_3 solutions to CaF_2 powders at acidic condition, followed by a hydrothermal treatment

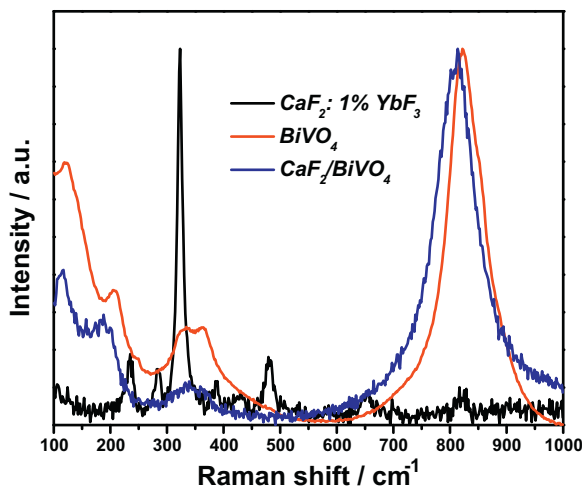


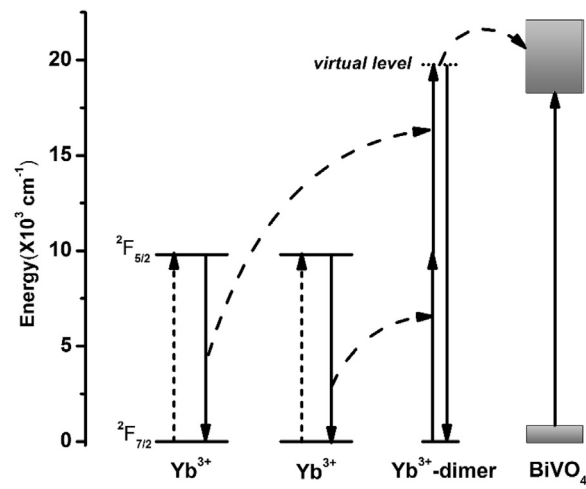
Fig. 3. Raman spectra of CaF_2 :Yb, BiVO_4 and CaF_2 :Yb@ BiVO_4 composite.

at 160°C for 24 h, a number of small sized particles were found to deposit on the CaF_2 particles (Fig. 2b and c). As shown in the XRD pattern (Fig. 1), these nanoparticles are composed of monoclinic phased BiVO_4 corresponding to the JCPDS file NO. 14-0688, while CaF_2 still maintains the cubic structure. It is noted that a few neighboring diffraction peaks are merged into a broad peak, indicating a small size of BiVO_4 particles. The EDX spectrum shown in Fig. 2 reveals that the CaF_2 :Yb sample deposited with BiVO_4 consists of Ca, Yb, F, Bi, V, and O (Fig. 2(e)), corresponding to the composition of CaF_2 and BiVO_4 , while the sample composed of CaF_2 :Yb alone consists of Ca, F, and Yb (Fig. 2(d)).

Fig. 3 shows the Raman spectra of individual CaF_2 :Yb and BiVO_4 , and CaF_2 @ BiVO_4 composite. For CaF_2 :Yb alone, several peaks located at 235, 324, 385, 482 and 656 cm^{-1} are observed, which are attributed to the vibration mode of CaF_2 [44,45]. Upon the deposition of BiVO_4 nanoparticles onto CaF_2 particles, additional vibration peaks at 121, 207, 327, 364 and 821 cm^{-1} appears, which belong to characteristic vibrational modes of BiVO_4 [46]. Among them, the vibration peak at 821 cm^{-1} is the strongest, corresponding to the symmetric stretching vibration of vanadate units. It is worth noting that the Raman peaks of BiVO_4 in the composite is red-shifted, compared with those of BiVO_4 alone, indicating the formation of CaF_2 @ BiVO_4 composite. The photoluminescence characterization of resulting product provides further evidence of the successful deposition of BiVO_4 nanoparticles on the CaF_2 particles (see below).

3.2. Photoluminescence and energy transfer

CaF_2 :1% Yb^{3+} is a typical cooperative luminescence material. In Yb^{3+} -doped CaF_2 host, Yb^{3+} ions substitute for Ca^{2+} ions and are situated in nearly tetragonal crystal-field environments. At 1-mol% dopant concentration, Yb^{3+} ions doped into CaF_2 prefer to form the clusters [43]. Under the pumping of a NIR laser, a pair of Yb^{3+} ions (a Yb^{3+} -dimer) were both exited from $^2\text{F}_{7/2}$ to $^2\text{F}_{5/2}$ level, and then depopulated from excited state $^2\text{F}_{5/2}$ simultaneously to emit a visible photon, which is called as cooperative luminescence (see Scheme 1). Fig. 4 shows the photoluminescence spectrum of CaF_2 :1% Yb^{3+} under 980 nm excitation. We can see a broad band ranging from 470 to 570 nm, which originates from the cooperative luminescence of Yb^{3+} -dimers. It is found that this broad band is composed of a few sharp emission peaks that are connected with each other. It is well known that the $^2\text{F}_{5/2}$ to $^2\text{F}_{7/2}$ levels of Yb^{3+} ions split into three and four Stark components in a tetragonal crystal field, respectively [47]. Therefore, a random combination



Scheme 1. Cooperative luminescence of a Yb^{3+} -dimer in CaF_2 host and cooperative sensitization of BiVO_4 by a Yb^{3+} -dimer.

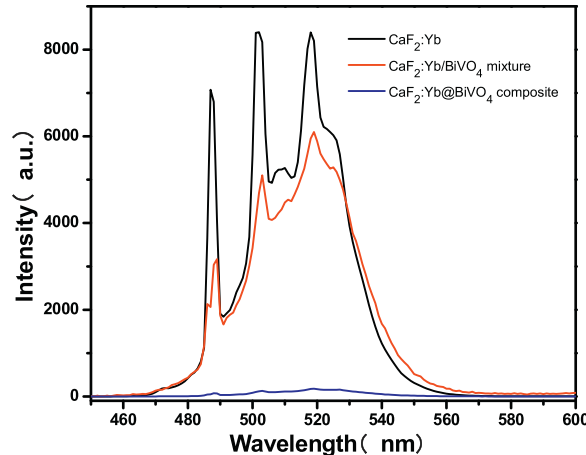


Fig. 4. Photoluminescence (PL) spectra of CaF_2 :1% Yb^{3+} , a physical mixture of CaF_2 :1% Yb^{3+} and BiVO_4 , CaF_2 :1% Yb^{3+} @ BiVO_4 composite under 980 nm excitation at room temperature.

of two Stark components in cooperative luminescence of a Yb^{3+} -dimer forms an emission located at different energies but close to each other [43]. These approaching emission peaks are connected to form a broad band.

After depositing BiVO_4 nanoparticles onto the surface of CaF_2 :Yb particles, the remarkable spectral difference can be observed (Fig. 4). The emission of CaF_2 :Yb nearly disappears. For comparison, the physical mixture of CaF_2 :Yb and BiVO_4 was also prepared by mixing both of them via grinding. The emission of CaF_2 :Yb shows a slight decrease for the CaF_2 :Yb/ BiVO_4 mixture (Fig. 4).

To ascertain the origin of the above spectral difference, the UV-vis-NIR absorption of CaF_2 :Yb@ BiVO_4 composites was measured and recorded in Fig. 5. In the spectrum, except for the absorption of Yb^{3+} around 980 nm (inset), a well-defined absorption band starting at $\sim 540\text{ nm}$ was observed, corresponding to the bandgap absorption of semiconductor BiVO_4 [48]. Therefore we can speculate that the visible photon energy generated via a cooperative luminescence process of Yb^{3+} -dimers can be absorbed by semiconductor BiVO_4 via an energy transfer between them for the sample CaF_2 :Yb@ BiVO_4 . But for the CaF_2 :Yb/ BiVO_4 mixture, the energy transfer between CaF_2 :Yb and BiVO_4 is difficult to take place due to a large distance between them.

Such a conclusion was further supported by the fluorescence dynamic analysis of Yb^{3+} . The fluorescence dynamic curves of

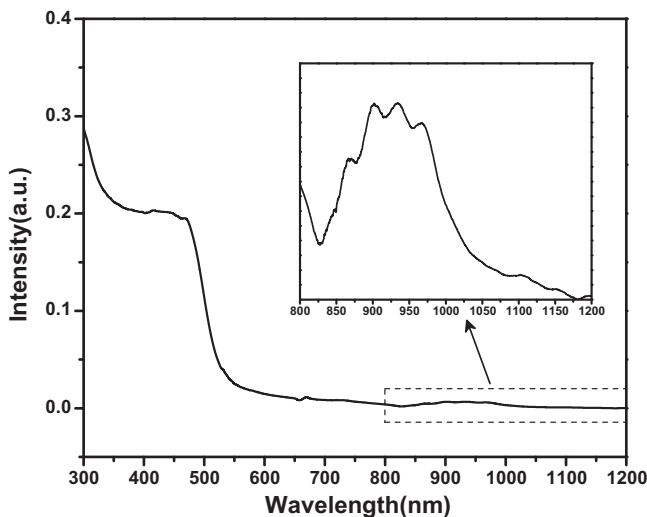


Fig. 5. UV-vis-NIR absorption spectra of $\text{CaF}_2\text{:Yb@BiVO}_4$ composite.

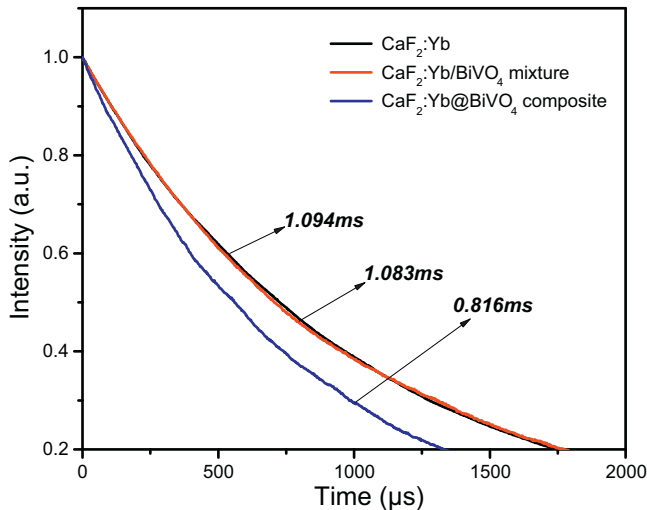


Fig. 6. Luminescence dynamic curves of Yb^{3+} -dimers in $\text{CaF}_2\text{:Yb}$, $\text{CaF}_2\text{:Yb/BiVO}_4$ mixture and $\text{CaF}_2\text{:Yb@BiVO}_4$ composite under 978 nm excitation.

Yb^{3+} -dimer emission (521 nm) were recorded under excitation of a 978 nm laser for the samples $\text{CaF}_2\text{:Yb}$, $\text{CaF}_2\text{:Yb@BiVO}_4$ composite and $\text{CaF}_2\text{:Yb/BiVO}_4$ mixture, as shown in Fig. 6. For $\text{CaF}_2\text{:Yb}$ alone, the lifetime of cooperative excited state of a Yb^{3+} -dimer is long with ~ 1.094 ms. The long-lived excited state of lanthanide ions ensures an efficient energy transfer to semiconductor. As observed, the decay time of the Yb^{3+} -dimer excited level decreased to 0.816 ms in the $\text{CaF}_2\text{:Yb@BiVO}_4$ composite, while almost no change was observed for the $\text{CaF}_2\text{:Yb/BiVO}_4$ mixture (1.083 ms), compared with that of $\text{CaF}_2\text{:Yb}$. It is reasonable to infer that the energy of the excited state of Yb^{3+} -dimer can be transferred directly to semiconductor BiVO_4 in the $\text{CaF}_2\text{:Yb@BiVO}_4$ composite, since the cooperative excited energy of a Yb^{3+} -dimer in CaF_2 overlaps well with the bandgap of semiconductor BiVO_4 (see Scheme 1). Such energy transfer behavior was also observed in our previously reported $\text{NaYF}_4\text{:Yb,Tm@TiO}_2$ and $\text{NaYF}_4\text{:Yb,Tm@ZnO}$ systems [32,49].

As we know, the lifetime of an excited state, τ , is determined by the radiative transition rate (W_R), the nonradiative transition rate (W_{NR}), and the energy transfer rate (W_{ET}), which can be expressed as $\tau = 1/(W_R + W_{NR} + W_{ET})$ [49,50]. The presence of BiVO_4 deposited on the $\text{CaF}_2\text{:Yb}$ particle surface creates nonradiative energy trans-

fer channels from the cooperative excited state of a Yb^{3+} -dimer to BiVO_4 . Such additional energy transfer process obviously accelerates the relaxation of the excited states of Yb^{3+} -dimers, resulting in the increase of overall transition rates and thus the reduction of fluorescence lifetime. The shortening of fluorescence lifetime of Yb^{3+} -dimers in the $\text{CaF}_2\text{:Yb@BiVO}_4$ composite indicates that the energy migration between $\text{CaF}_2\text{:Yb}$ and BiVO_4 is dominated by a fluorescence resonance energy transfer (FRET) process, rather than by a radiation-reabsorption process, because the fluorescence lifetime of the donor is unchanged in the latter process. Therefore, the cooperative energy of the excited states of a Yb^{3+} -dimer is transferred directly to semiconductor BiVO_4 , leading to a significant decrease of the emission of Yb^{3+} -dimers (Fig. 4). For the $\text{CaF}_2\text{:Yb/BiVO}_4$ mixture, the lifetime of excited state of Yb^{3+} -dimer is almost unchanged, compared with that for the sample $\text{CaF}_2\text{:Yb}$, indicating a radiation-reabsorption process for the energy transfer from $\text{CaF}_2\text{:Yb}$ to BiVO_4 . Moreover, the energy transfer is inefficient due to a relatively large distance between $\text{CaF}_2\text{:Yb}$ and BiVO_4 in the $\text{CaF}_2\text{:Yb/BiVO}_4$ mixture, corresponding to a slight decrease of Yb^{3+} -dimer emission (Fig. 4). Indeed, the difference of the energy transfer mechanism affects the photocatalytic activity of BiVO_4 significantly, which will be discussed in the section below.

3.3. Photocatalytic activity

As discussed earlier, the n-type semiconductor BiVO_4 is activated mainly by the energy transfer from excited Yb^{3+} -dimers via a FRET process in the $\text{CaF}_2\text{:Yb@BiVO}_4$ composite. Thus, the electrons and holes are generated in the conduction band (CB) and the valence band (VB), respectively, and then these electron–hole pairs migrate from the inner region to the surfaces to take part in surface reactions. The separated electrons and holes arriving on the surface react with O_2 and H_2O to generate $\cdot\text{OH}$ and $\text{O}_2\cdot$. These reactive oxygen species with strong oxidation ability can oxidize pollutant molecules and perform photocatalysis [51–54].

Methylene blue (MB) compound as a model pollutant was used to investigate the photocatalytic activity of the $\text{CaF}_2\text{:Yb@BiVO}_4$ composite under NIR irradiation of 980 nm. 0.5 mg of $\text{CaF}_2\text{:Yb@BiVO}_4$ particles was dispersed into a quartz cuvette containing 0.5 mL of MB aqueous solution (15 mg L^{-1}). For comparing the photocatalytic activity, the concentrations of the catalyst and pollutant and NIR irradiation power used in this work are the same as those in our previous work [32]. Prior to the photocatalysis experiment, the dark reaction of MB in the presence of catalysts was conducted to establish adsorption/desorption equilibrium of MB on the surfaces of $\text{CaF}_2\text{:Yb@BiVO}_4$ particles.

Fig. 7(a) shows the absorbance spectra of MB catalyzed by the $\text{CaF}_2\text{:Yb@BiVO}_4$ particles under 980 nm irradiation as a function of irradiation time. The absorbance band around 664 nm is characteristic of MB. We can see that the absorbance of MB decreases gradually with an increase of irradiation time, indicating the degradation of MB upon NIR irradiation. The photocatalytic activity of $\text{CaF}_2\text{:Yb@BiVO}_4$ can be evaluated through the concentration of MB after NIR irradiation relative to original one of MB. Fig. 7(b) shows the time dependent ratios of C/C_0 , where C_0 is the original concentration of MB and C is the concentration of MB irradiated with a 980 nm laser for time t . C can be calibrated by comparing the absorption of the MB solution with that of the standard MB solution at a wavelength of 664 nm. Thus, the value of C/C_0 stands for the degradation degree of MB. We can see from Fig. 7(b) that the degradation ratio of MB increases continuously with the irradiation time and reached about 80% after 7 h of irradiation in the presence of $\text{CaF}_2\text{:Yb@BiVO}_4$ particles. This new type of NIR photocatalyst presented here seems efficient, compared with our previously reported

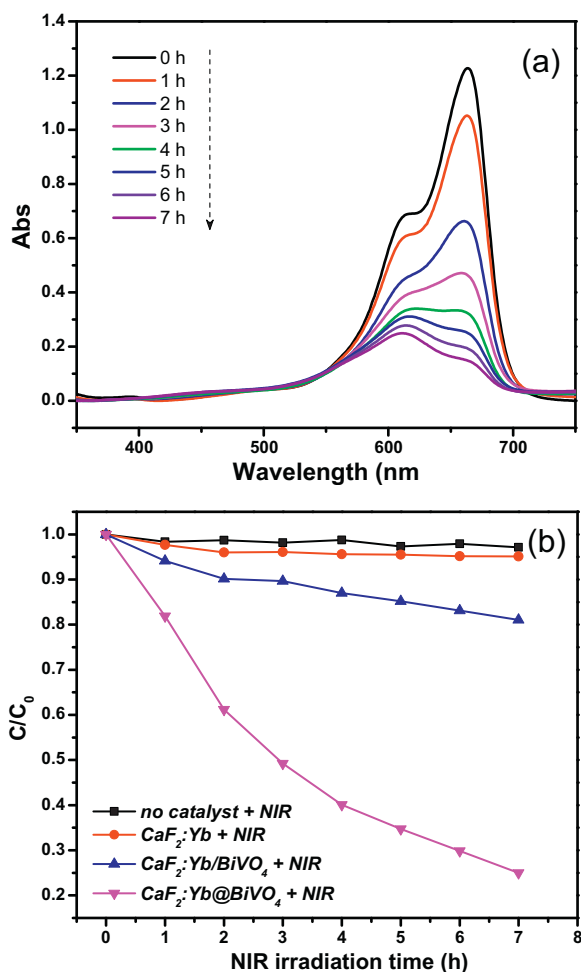


Fig. 7. (a) Absorbance spectra of MB catalyzed by CaF₂:Yb@BiVO₄ photocatalyst at different irradiation times under 980 nm excitation; (b) the time dependent ratios of C/C_0 in the presence of CaF₂:Yb, CaF₂:Yb@BiVO₄ composite and CaF₂:Yb@BiVO₄ mixture.

NaYF₄:Yb,Tm@TiO₂ system, since only 65% of degradation ratio was achieved with 14 h of NIR irradiation for the latter [32].

To get an optimum ratio of CaF₂:Yb to BiVO₄, we prepared the CaF₂:Yb@BiVO₄ composites with different CaF₂:Yb-to-BiVO₄ molar ratios (10:0, 5, 10:1, 10:2, 10:3, 10:4, respectively). The photocatalysis was performed with NIR irradiation for these composites, as shown in Fig. S1 (Supplementary Information). We can see that the most highest photocatalytic activity is obtained for the composite with CaF₂:Yb-to-BiVO₄ molar ratio of 10:2. Therefore, the composite with CaF₂ to BiVO₄ molar ratio of 10:2 was chosen for the following discussion.

In our previously reported NaYF₄:Yb,Tm@TiO₂ system, a two-step energy transfer of $\text{Yb}^{3+} \rightarrow \text{Tm}^{3+} \rightarrow \text{TiO}_2$ was involved to realize NIR photocatalysis so that the ultimate photo quantum yield for exciting TiO₂ might be very low [32]. Another example involving two-step energy transfer for NIR photocatalysis is the photocatalyst BiVO₄/CaF₂:Er³⁺,Tm³⁺,Yb³⁺, in which the successive energy transfer from Yb^{3+} to Tm^{3+} occurs first, and then the excited Tm^{3+} transfer its energy to BiVO₄ [53]. In comparison, only a one-step energy transfer of Yb^{3+} -dimers \rightarrow BiVO₄ occurs for NIR photocatalysis in our present photocatalytic CaF₂:Yb@BiVO₄ system. The reduction of energy transfer procedures might be responsible for the improvement of photocatalytic activity.

To demonstrate the origin of MB degradation upon NIR irradiation in the presence of CaF₂:Yb@BiVO₄ particles, the parallel experiments were performed as follows. (i) To examine whether photolysis of MB occur under NIR irradiation, MB solution was

irradiated with a NIR laser in the absence of CaF₂:Yb and BiVO₄. In this case, almost no degradation of MB occurred. (ii) To examine whether thermal degradation of MB occur, MB solution was irradiated with NIR light in the presence of CaF₂:Yb, and almost no MB degradation was observed. As we know, both NIR irradiation and nonradiative relaxations of excited Yb^{3+} ions can generate thermal energy. Therefore, The temperature of MB solution was recorded with time upon 980 nm irradiation in the presence of CaF₂:Yb. The temperature variation is limited with an increase from 12 °C to 40 °C, which is not enough to cause thermal degradation of MB significantly. The above control experiments indicate that the degradation of MB under NIR irradiation in the presence of CaF₂:Yb@BiVO₄ is caused mostly by photocatalysis, rather than by photolysis or thermal degradation.

For comparing the difference in the photocatalytic activities for the CaF₂:Yb@BiVO₄ composite and CaF₂:Yb/BiVO₄ mixture (the same CaF₂-to-BiVO₄ molar ratio as that in the composite), MB solution was irradiated by NIR light in the presence of CaF₂:Yb/BiVO₄ mixture, and 18% of MB was found to be decomposed within 7 h, which is four times lower than the case of CaF₂:Yb@BiVO₄ composite (~80%). This could be attributed to the difference of their energy migration routes, as has been discussed in the 'Photoluminescence' section. In the CaF₂:Yb@BiVO₄ composite, CaF₂:Yb and BiVO₄ particles attach closely to each other and form compact interfaces, which benefits FRET processes. Moreover, the energy transfer rate from excited Yb-dimers to BiVO₄ is larger than the spontaneous radiative transition rate, leading to a high excitation efficiency of BiVO₄ by NIR photons via a FRET process. Therefore, in the CaF₂:Yb@BiVO₄ composite, a relatively high photon quantum yield can be achieved to activate BiVO₄, resulting in a relatively high photocatalytic activity. In contrast, there are no contact interfaces between CaF₂:Yb and BiVO₄ particles in the CaF₂:Yb/BiVO₄ mixture, and thus BiVO₄ can be excited via a radiation-reabsorption process. The radiation-reabsorption efficiency is low due to a large distance between CaF₂:Yb and BiVO₄ particles, finally resulting in a low photocatalytic activity. These results indicate that FRET is an important mechanism in the NIR photocatalytic activity.

In addition to high photocatalytic activity, the photochemical stability and reproducibility are also important factors in the practical applications. The stability and durability of CaF₂:Yb@BiVO₄ composites are assessed by performing recycling experiments, as shown in Fig. 8. No obvious loss in the activity can be observed after five cycles, indicating the CaF₂:Yb@BiVO₄ composite is stable and not corroded in spite of a long time of NIR irradiation.

4. Conclusions

The powder sample of CaF₂:1%Yb³⁺ was prepared using a high temperature solid-state reaction method, and BiVO₄ nanoparticles were deposited on the surface of CaF₂:1%Yb³⁺ powders by a hydrothermal method. XRD, TEM, EDX, Raman and PL spectral analysis revealed that BiVO₄ nanocrystals were attached around CaF₂:1%Yb³⁺ particles, forming CaF₂:1%Yb³⁺@BiVO₄ composites. Under excitation of a 980 nm laser, CaF₂:1%Yb³⁺ emits bright green light via cooperative luminescence of Yb³⁺-dimers. In the CaF₂:1%Yb³⁺@BiVO₄ composite, cooperative energy transfer of a Yb³⁺-dimer to BiVO₄ take places under NIR excitation, leading to an indirect excitation of BiVO₄ by NIR light via a one-step energy transfer, as indicated by steady-state and dynamic fluorescence spectroscopy. The degradation of MB exposed to CaF₂:1%Yb³⁺@BiVO₄ composites upon NIR radiation demonstrated the NIR-driven photocatalytic capability. It is noteworthy that our present catalytic system CaF₂:1%Yb³⁺@BiVO₄ exhibits high photocatalytic activity with a nearly 80% degradation ratio of MB in 7 h of NIR light irradiation, compared with that of our previously

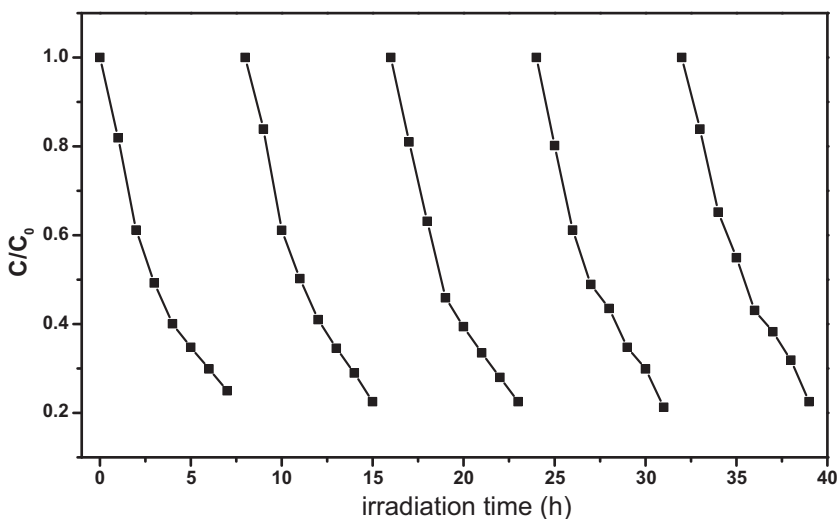


Fig. 8. The time dependent C/C_0 in the presence of $\text{CaF}_2:\text{Yb}@\text{BiVO}_4$ composite under 980 nm excitation during five repeated photocatalytic cycles.

reported systems ($\text{NaYF}_4:\text{Yb}$, $\text{Tm}@\text{TiO}_2$), for which $\sim 65\%$ of degradation ratio of MB was obtained within 14 h of NIR irradiation. No obvious loss in the activity can be observed after five photocatalysis cycles, indicating a good photochemical stability.

Acknowledgments

This work was supported by the National Natural Science Foundation of China (NSFC) (Grant Nos 11474132, 61178073).

Appendix A. Supplementary data

Supplementary data associated with this article can be found, in the online version, at <http://dx.doi.org/10.1016/j.apcatb.2016.12.027>.

References

- [1] M.R. Hoffmann, S.T. Martin, W. Choi, D.W. Bahnemann, *Chem. Rev.* 95 (1995) 69–96.
- [2] M.A. Garcia, J.M. Merino, E.F. Pinel, A. Quesada, J. Venta, M.L.R. Gonzalez, G.R. Castro, P. Crespo, J. Llopis, J.M. Gonzalez-Callbet, A. Hernando, *Nano Lett.* 7 (2007) 1489–1494.
- [3] J.G. Yu, X.X. Yu, *Environ. Sci. Technol.* 42 (2008) 4902–4907.
- [4] Y.M. Lin, D.Z. Li, J.H. Hu, G.C. Xiao, J.X. Wang, W.J. Li, X.Z. Fu, *J. Phys. Chem. C* 116 (2012) 5764–5772.
- [5] H. Choi, Y.J. Kim, R.S. Varma, D.D. Dionysiou, *Chem. Mater.* 18 (2006) 5377–5384.
- [6] A. Fujishima, K. Honda, *Nature* 238 (1972) 37–38.
- [7] B. O'Regan, M. Grätzel, *Nature* 353 (1991) 737–740.
- [8] M. Grätzel, *Nature* 414 (2001) 338–344.
- [9] X. Chen, S.S. Mao, *Chem. Rev.* 107 (2007) 2891–2959.
- [10] Q. Zhu, J.S. Qian, H. Pan, L. Tu, X.F. Zhou, *Nanotechnology* 22 (2011) 395703.
- [11] D. Tsukamoto, A. Shiro, Y. Shiraishi, Y. Sugano, S. Ichikawa, S. Tanaka, T. Hirai, *ACS Catal.* 2 (2012) 559–603.
- [12] C.B.D. Marien, T. Cottineau, D. Robert, P. Drogui, *Appl. Catal. B: Environ.* 194 (2016) 1–6.
- [13] H. Sun, D.J. Mowbray, A. Migani, J. Zhao, H. Petek, A. Rubio, *ACS Catal.* 5 (2015) 4242–4254.
- [14] R. Sigh, R. Bapat, L.J. Qin, H. Feng, V. Polshettiwar, *ACS Catal.* 6 (2016) 2770–2784.
- [15] H. Aita, N. Hori, M. Takeuchi, T. Suzuki, M. Yamada, *Biomaterials* 30 (2009) 1015–1025.
- [16] A. Amtout, R. Leonelli, *Phys. Rev. B* 51 (1995) 6842–6851.
- [17] W.J. Wang, Y.C. Li, Z.W. Kang, F. Wang, J.C. Yu, *Appl. Catal. B: Environ.* 182 (2016) 184–192.
- [18] Z.H. Xu, M. Quintanilla, F. Vetrone, A.O. Govorov, M. Chaker, D.L. Ma, *Adv. Funct. Mater.* 25 (2015) 2950–2960.
- [19] R. Asahi, T. Morikawa, T. Ohwaki, K. Aoki, Y. Taga, *Science* 293 (2001) 269–271.
- [20] Y. Izumi, T. Itoi, S. Peng, K. Oka, Y. Shibata, *J. Phys. Chem. C* 113 (2009) 6706–6718.
- [21] J. Zhang, Y. Wu, M. Xing, S.A.K. Leghari, S. Sajjad, *Energy Environ. Sci.* 3 (2010) 715–726.
- [22] G.L. Huang, Y.F. Zhu, *J. Phys. Chem. C* 111 (2007) 11952–11958.
- [23] N. Murakami, A. Ono, M. Nakamura, T. Tsubota, T. Ohno, *Appl. Catal. B: Environ.* 97 (2010) 115–119.
- [24] M. Pelaez, N.T. Nolan, S.C. Pillai, M.K. Seery, P. Falaras, A.G. Kontos, P.S.M. Dunlop, J.W.J. Hamilton, J.A. Byrne, K.O. Shea, M.H. Entezari, D.D. Dionysiou, *Appl. Catal. B: Environ.* 125 (2012) 331–349.
- [25] D. Behar, J. Rabani, *J. Phys. Chem. B* 110 (2006) 8750–8755.
- [26] H.W. Huang, X.W. Li, J.J. Wang, F. Dong, P.K. Chu, T.R. Zhang, Y.H. Zhang, *ACS Catal.* 5 (2015) 4094–4103.
- [27] H. Choi, D. Shin, B.C. Yeo, T. Song, S.S. Han, N. Park, S. Kim, *ACS Catal.* 6 (2016) 2745–2753.
- [28] W. Choi, A. Termin, M.R. Hoffmann, *J. Phys. Chem.* 98 (1994) 13669–13679.
- [29] L. Xu, E.M.P. Steinmiller, S.E. Skrabalak, *J. Phys. Chem. C* 116 (2012) 871–877.
- [30] H. Chuang, D.H. Chen, *Nanotechnology* 20 (2009) 105704.
- [31] W.P. Qin, D.S. Zhang, D. Zhao, L.L. Wang, K.Z. Zheng, *Chem. Commun.* 46 (2010) 2304–2306.
- [32] Y.N. Tang, W.H. Di, X.S. Zhai, R.Y. Yang, W.P. Qin, *ACS Catal.* 3 (2013) 405–412.
- [33] C.K. Chen, H.M. Chen, C.J. Chen, R.S. Liu, *Chem. Commun.* 49 (2013) 7917–7919.
- [34] F. Gonell, M. Haro, R.S. Sanchez, P. Negro, I. Mora-Sero, J. Bisquert, B. Julian-Lopez, S. Gimenez, *J. Phys. Chem. C* 118 (2014) 11279–11284.
- [35] T.H. Yu, Y. Xuan, X.F. Wang, X.H. Yan, *RSC Adv.* 4 (2014) 49415–49420.
- [36] H. Jia, S.H. Zheng, C. Xu, W.B. Chen, J.C. Wang, X.F. Liu, J.R. Qiu, *Adv. Energy Mater.* 5 (2015) 1401041.
- [37] Z.Y. Hou, Y.X. Zhang, K.R. Deng, Y.Y. Chen, X.J. Li, X.R. Deng, Z.Y. Cheng, H.Z. Lian, C.X. Li, J. Lin, *ACS Nano* 9 (2015) 2584–2599.
- [38] Z.Y. Yu, Q.Q. Sun, W. Pan, N. Li, B. Tang, *ACS Nano* 9 (2015) 11064–11074.
- [39] L.Y. Zeng, Y.W. Pan, Y. Tian, X. Wang, W.Z. Ren, S.J. Wang, G.M. Lu, A.G. Wu, *Biomaterials* 57 (2015) 93–106.
- [40] E. Nakazawa, S. Shionoya, *Phys. Rev. Lett.* 25 (1970) 1710–1712.
- [41] M.P. Hehlen, A. Kudritcher, S.C. Rand, S.R. Luthi, *Phys. Rev. Lett.* 82 (1999) 3050–3053.
- [42] P. Goldner, B. Schaudel, M. Prassas, *Phys. Rev. B* 65 (2002) 054103.
- [43] W.P. Qin, Y.Z. Liu, C.N. Sin, C.F. Wu, G.S. Qin, Z. Chen, K.Z. Zheng, *Light Sci. Appl.* 3 (2014) e193.
- [44] D.L. Wood, W. Kaiser, *Phys. Rev.* 126 (1962) 2079–2088.
- [45] J.P. Russ, *Proc. Phys. Soc.* 85 (1965) 194–196.
- [46] P. Madhusudan, J.R. Ran, J. Zhang, J.G. Yu, G. Liu, *Appl. Catal. B: Environ.* 110 (2011) 286–295.
- [47] M.J. Weber, R.W. Bierig, *Phys. Rev. B* 134 (1964) A1492.
- [48] O.F. Lopes, K.T.G. Carvalho, A.E. Nogueira, W. Avansi Jr., C. Ribeiro, *Appl. Catal. B: Environ.* 188 (2016) 87–97.
- [49] X.Y. Guo, W.Y. Song, C.F. Chen, W.H. Di, W.P. Qin, *Phys. Chem. Chem. Phys.* 15 (2013) 14681–14688.
- [50] W.H. Di, X.J. Wang, B.J. Chen, S.Z. Lv, X.X. Zhao, *J. Phys. Chem. B* 109 (2005) 13154–13158.
- [51] A. Houas, H. Lachheb, M. Ksibi, E. Elaloui, C. Guillard, J.M. Hermann, *Appl. Catal. B: Environ.* 31 (2001) 145–157.
- [52] Z. Dai, F. Qin, H.P. Zhao, J. Ding, Y.L. Liu, R. Chen, *ACS Catal.* 6 (2016) 3180–3192.
- [53] S.Q. Huang, N.W. Zhu, Z.Y. Lou, L. Gu, C. Miao, H.P. Yuan, A.D. Shan, *Nanoscale* 6 (2016) 1362–1368.
- [54] S.Q. Huang, Z.Y. Lou, Z.B. Qi, N.W. Zhu, H.P. Yuan, *Appl. Catal. B: Environ.* 168 (2015) 313–321.